



## Article

# Ultraviolet-Ozone Treatment: An Effective Method for Fine-Tuning Optical and Electrical Properties of Suspended and Substrate-Supported MoS<sub>2</sub>

Fahrettin Sarcan <sup>1,2,\*</sup> , Alex J. Armstrong <sup>1</sup> , Yusuf K. Bostan <sup>2,3</sup>, Esra Kus <sup>2</sup>, Keith P. McKenna <sup>1</sup>, Ayse Erol <sup>2</sup> and Yue Wang <sup>1,\*</sup>

- <sup>1</sup> School of Physics, Engineering and Technology, University of York, Heslington, York YO10 5DD, UK; alex.armstrong@york.ac.uk (A.J.A.); keith.mckenna@york.ac.uk (K.P.M.)
- <sup>2</sup> Department of Physics, Faculty of Science, Istanbul University, Vezneciler, Istanbul 34134, Turkey; yusufkerembostan@gmail.com (Y.K.B.); esraakus2021@gmail.com (E.K.); ayseerol@istanbul.edu.tr (A.E.)
- <sup>3</sup> Institut d'Electronique, Microelectronique & Nanotechnologie IEMN CNRS UMR 8520, Université Polytechnique Hauts de France, 59313 Valenciennes, France
- \* Correspondence: fahrettin.sarcan@istanbul.edu.tr (F.S.); yue.wang@york.ac.uk (Y.W.)

**Abstract:** Ultraviolet-ozone (UV-O<sub>3</sub>) treatment is a simple but effective technique for surface cleaning, surface sterilization, doping, and oxidation, and is applicable to a wide range of materials. In this study, we investigated how UV-O<sub>3</sub> treatment affects the optical and electrical properties of molybdenum disulfide (MoS<sub>2</sub>), with and without the presence of a dielectric substrate. We performed detailed photoluminescence (PL) measurements on 1–7 layers of MoS<sub>2</sub> with up to 8 min of UV-O<sub>3</sub> exposure. Density functional theory (DFT) calculations were carried out to provide insight into oxygen-MoS<sub>2</sub> interaction mechanisms. Our results showed that the influence of UV-O<sub>3</sub> treatment on PL depends on whether the substrate is present, as well as the number of layers. Additionally, 4 min of UV-O<sub>3</sub> treatment was found to be optimal to produce p-type MoS<sub>2</sub>, while maintaining above 80% of the PL intensity and the emission wavelength, compared to pristine flakes (intrinsically n-type). UV-O<sub>3</sub> treatment for more than 6 min not only caused a reduction in the electron density but also deteriorated the hole-dominated transport. It is revealed that the substrate plays a critical role in the manipulation of the electrical and optical properties of MoS<sub>2</sub>, which should be considered in future device fabrication and applications.

**Keywords:** MoS<sub>2</sub>; ultraviolet-ozone (UV-O<sub>3</sub>); doping; surface treatment; transition metal dichalcogenide; field-effect transistor; photoluminescence; density functional theory (DFT)



**Citation:** Sarcan, F.; Armstrong, A.J.; Bostan, Y.K.; Kus, E.; McKenna, K.P.; Erol, A.; Wang, Y. Ultraviolet-Ozone Treatment: An Effective Method for Fine-Tuning Optical and Electrical Properties of Suspended and Substrate-Supported MoS<sub>2</sub>.

*Nanomaterials* **2023**, *13*, 3034. <https://doi.org/10.3390/nano13233034>

Academic Editor: Silvia Villar-Rodil

Received: 21 October 2023

Revised: 23 November 2023

Accepted: 24 November 2023

Published: 27 November 2023



**Copyright:** © 2023 by the authors. Licensee MDPI, Basel, Switzerland. This article is an open access article distributed under the terms and conditions of the Creative Commons Attribution (CC BY) license (<https://creativecommons.org/licenses/by/4.0/>).

## 1. Introduction

In recent years, semiconducting two-dimensional transition metal dichalcogenides (2D-TMDs) have become a group of highly demanded materials for next-generation optoelectronic devices such as photodetectors and light emitters [1–4] because of their unique optical, electronic, and structural properties. Despite many advantages of these semiconducting materials, there are some drawbacks such as low carrier concentration and mobility, which result in low electrical conductivity [5,6] compared to the materials already widely used in electronic/optoelectronic technologies, such as Si and GaAs. To realize high-performance optoelectronic devices, both n-type and p-type semiconducting 2D-TMDs are required [7,8]. Conventional doping techniques used for semiconductors are not suitable for 2D materials because they modify their crystal structures and result in a significant deterioration of their optoelectrical properties [9]. On the other hand, thanks to the atomic thickness of 2D-TMDs, their optical and structural properties as well as carrier dynamics can be efficiently engineered using different post-growth methods [10]. Surface charge transfer-based doping [11], substitutional doping [12], interstitial doping [13], and

vacancy-based doping [14] are the main post-growth doping mechanisms for 2D-TMDs [15]. Based on these mechanisms, there are several reported doping techniques such as chemical treatment [13], ion implantation [16], plasma doping [17], thermal annealing [18], electron beam irradiation [19], and ultraviolet-ozone (UV-O<sub>3</sub>) treatment [20], which aim to achieve n- and/or p-type doping. Due to the high sensitivity of 2D materials' properties, the main challenge in post-growth doping is to maintain their superb optoelectrical properties for device applications, while controlling the doping concentration with consistency. In this study, we focus on the effect of UV-O<sub>3</sub> treatment on the optical and electrical properties of MoS<sub>2</sub>, which leads to p-type doping of the TMD material.

UV-O<sub>3</sub> treatment is a useful process for a wide range of materials for surface modification [21]. It has been employed as an effective tool for defect engineering and doping in graphene and 2D TMDs. There are a few studies in the literature on UV-O<sub>3</sub>-induced p-type doping on graphene [22–24]. Liang et al. presented controllable p-type doping in a range of semiconducting TMDs (MoTe<sub>2</sub>, WSe<sub>2</sub>, MoSe<sub>2</sub>, and PtSe<sub>2</sub>) and proposed three mechanisms for UV-O<sub>3</sub>-induced hole doping: (1) charge transfer due to the interaction with oxygen molecules, (2) isoelectronic substitution of chalcogen atoms with oxygen atoms, and (3) charge transport over the oxide surface due to the transition metal oxide formation (MoO<sub>3</sub>, WO<sub>3</sub> etc.) [20]. Zheng et al. showed that UV-O<sub>3</sub> treatment is an effective method for p-type doping of MoTe<sub>2</sub> field-effect transistors and it enhances its electrical performance enormously. The hole concentration and mobility are enhanced by nearly two orders of magnitude, and the conductivity by five orders of magnitude [25]. These promising studies are focused on the effect of UV-O<sub>3</sub> treatment on the electrical properties of TMDs only. In 2D-TMD optoelectronic devices, the effect of UV-O<sub>3</sub> treatment on their optical properties is also critical. There are only a few studies about the effect of UV-O<sub>3</sub> treatment on the optical properties of semiconducting TMDs. Yang et al. reported that PL intensity of pristine exfoliated MoS<sub>2</sub> decreased and was eventually quenched as UV-O<sub>3</sub> exposure time increased from 0 to 10 min, which was attributed to the structural degradation [26]. The quenching of PL was also observed on chemical vapour deposited and exfoliated monolayer MoS<sub>2</sub> [27] and on exfoliated monolayer WS<sub>2</sub> and WSe<sub>2</sub> as a result of 6 min of UV-O<sub>3</sub> treatment due to oxidation [28]. On the other hand, Zheng et al. showed a 37-fold increment in the PL intensity by converting trilayer MoSe<sub>2</sub> to monolayer with 7 min of UV-O<sub>3</sub> treatment [29]. While the effect of UV-O<sub>3</sub> on the electrical properties is consistent from one study to another, there is a contradiction about the effect of UV-O<sub>3</sub> treatment on the optical properties of 2D-TMDs. More importantly, there is no systematic study on the effect of UV-O<sub>3</sub> treatment on suspended, or multi-layer TMDs. Although monolayer (ML) TMDs have the strongest emission, the effect on few-layer TMDs is also important for the potential electronic and optoelectronic devices.

In this paper, we reveal that the effect of UV-O<sub>3</sub> treatment does not only depend on the type of materials but also the number of layers and the substrate (the environment). To investigate the layer and substrate dependency of the UV-O<sub>3</sub> treatment on the optical properties of semiconducting TMDs, we fabricated suspended and substrate-supported MoS<sub>2</sub> samples with different numbers of layers from monolayer to seven layers. PL spectroscopy was carried out to investigate the effect on their optical properties with a range of UV-O<sub>3</sub> exposure time. Density functional theory (DFT) calculations were performed to understand which oxygen-related mechanism during the UV-O<sub>3</sub> exposure could cause p-type doping via charge trapping, as well as the role of intrinsic sulphur defects. Further electrical characterisation was performed on a 4L-MoS<sub>2</sub> transistor to investigate how the carrier dynamics can be modified using the UV-O<sub>3</sub> treatment.

## 2. Experimental Methods

E-beam lithography was used to pattern the squares (4 μm × 4 μm) on Polymethyl methacrylate (PMMA)-coated Si<sub>3</sub>N<sub>4</sub> (150 nm)-on-SiO<sub>2</sub> substrates. Patterned squares were etched 300 nm in depth with a Reactive Ion Etcher, using a mixture gas of CHF<sub>3</sub> and O<sub>2</sub>. Resist was removed with a resist remover (1165) and acetone, and the substrate was rinsed

in isopropyl alcohol (IPA) before drying. Bulk single-crystal MoS<sub>2</sub> was purchased from HQ Graphene, which was intrinsically n-doped. Scotch tape and polydimethylsiloxane (PDMS)-assisted mechanical exfoliation method was used to obtain MoS<sub>2</sub> flakes with different numbers of layers. The flakes larger than 10 μm × 10 μm were transferred either onto the etched squares to be suspended or the flat area of the Si<sub>3</sub>N<sub>4</sub>-on-SiO<sub>2</sub> substrates.

The PL spectra of the flakes were measured using a microPL setup equipped with an Andor iDus detector and a 532 nm excitation laser, before and after UV-O<sub>3</sub> treatment. The laser beam was focused to be a spot of ~1.5 μm in diameter, fitting inside the suspended areas. The UV-O<sub>3</sub> treatment was performed (Jelight, 30 mW/cm<sup>2</sup> at a wavelength of 254 nm) for different periods of time.

DFT calculations were undertaken on four-layer MoS<sub>2</sub> using a plane wave basis set, as implemented in the VASP package [30–32]. A gamma-centred Monkhorst-Pack grid of 2 × 2 × 1 *k* points was used to sample the Brillouin zone for all calculations, with geometry optimizations performed to a force tolerance of 0.01 eV/Å. Ideal values of D3 parameters for HSE06 are still an open area of research and could therefore not be sourced from the literature, so in this study, we used parameters quoted for the related hybrid functional PBE0 for calculations. Version 5.2 PBE plane wave potentials (PAW) were used for all calculations, with a plane wave cut-off value of 520 eV.

Preliminary geometry optimizations were undertaken with the Perdew–Burke–Ernzerhof (PBE) functional [33], including Grimme’s D3 van der Waals corrections [34] to determine the lowest energy adsorption site and adsorbate bond orientations. Further calculations of the band structures, including substitutional defects, were undertaken using the HSE06 functional with D3 corrections, ensuring more accurate energy levels to fully capture any charge-trapping levels [35]. These calculations were initially optimized with one extra electron added to capture the geometry of the charged structure, then reoptimized for the neutral case. This enabled Bader charge analysis to be conducted on both neutral and charged cases to identify if the charged case differed greatly at the defect site, which would be indicative of charge trapping. To reduce the defect density and prevent bands forming from the defect levels, the unit cell used was double the size of the primitive cell in the *a* and *b* directions. A vacuum gap of 20 Å was employed to minimize interaction between periodically repeated slabs.

The band structure was also calculated for a pristine four-layer MoS<sub>2</sub> system at the HSE06 level, with the parameters described above and a high symmetry *k*-point path generated using the sumo package [36]. This was necessary to determine where the defect levels were relative to these bands. We note here that spin-orbit coupling was not included in any of these calculations; however, previous calculations on MoS<sub>2</sub> have shown this to result in a 0.1 eV shift in the band gap—significantly lower than the energy difference between the CBM and defect levels found in this work—hence it would be unlikely to change any conclusions [37].

Defect formation energies were calculated for each defect as a function of the chemical potential of sulphur to determine which defects were most stable under different conditions—from sulphur-poor to sulphur-rich. These energies were calculated using Equation (1), where  $\mu_i$  are the chemical potentials of species removed or added to the system and  $n_i$  is the change in the number of these atoms,  $i = \text{Mo, S or O}$ .

$$E_f^{\text{def}} = E^{\text{def}} - E^{\text{bulk}} - \sum n_i \mu_i \quad (1)$$

Both sulphur-rich and sulphur-poor limits were considered at a constant oxygen chemical potential—with only 2 points necessary due to the clear linear nature of these energies with respect to one chemical potential. These limits were defined as the sulphur chemical potential, where  $\mu_S = 1/2 E_{S_2}$  and  $\mu_{Mo} = E_{Mo}$  for the sulphur-rich and sulphur-poor cases, respectively, as either of these conditions uniquely defines both  $\mu_S$  and  $\mu_{Mo}$  according to Equation (2).

$$E_{\text{MoS}_2} = \mu_{\text{Mo}} + 2\mu_S \quad (2)$$

All energies used were calculated at PBE + D3 level of theory and the formation energies for O<sub>2</sub> defects were halved to calculate per oxygen atom and ensure these energies are comparable between the different systems.

Electronic states with enhanced localization on oxygen-related defects were identified by examining coefficients in the projection of one-electron wavefunctions onto atoms. To ensure the corresponding band energies were consistent between different supercells, the lowest energy molybdenum core state in the pristine surface was a reference for aligning electronic structures. The densities of states were calculated on a grid of 2000 points and plotted using the sumo package [36].

In order to monitor the doping effect with different UV-O<sub>3</sub> exposure times, a 4L-MoS<sub>2</sub> field-effect transistor was fabricated. A 4L MoS<sub>2</sub> flake was transferred on SiO<sub>2</sub>/Si wafer and e-beam lithography was used to pattern a Transfer Length Method (TLM) structure on the flake. Cr/Au (10 nm/60 nm) were deposited in a thermal evaporator, followed by a lift-off process. Electrical characterisation was carried out using an Agilent B2902A double-channel source-meter unit.

### 3. Results and Discussion

It is well known that the electronic band structure and energy bandgap of TMDs depend on the number of layers. The number of layers in MoS<sub>2</sub> flakes can be precisely determined using the PL peak wavelength/energy. Flakes with different layer numbers were selectively transferred to the pre-patterned Si<sub>3</sub>N<sub>4</sub> substrates. Figure 1a,b show a microscope image of the 4L MoS<sub>2</sub> flake on the Si<sub>3</sub>N<sub>4</sub> substrate, and a schematic drawing of the sample structure, respectively.

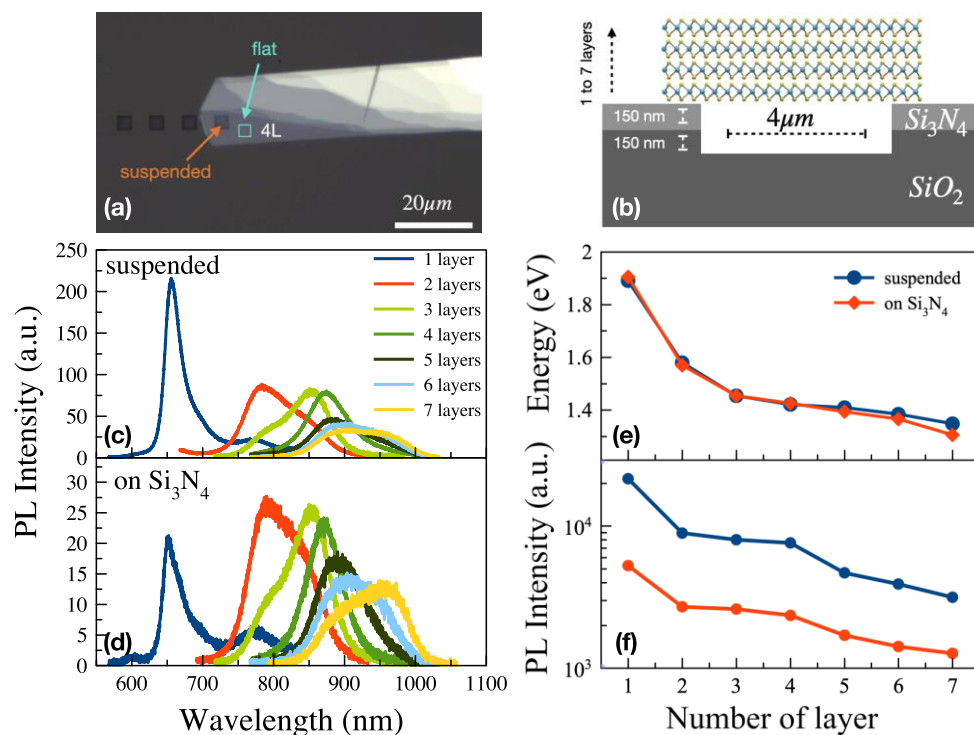


**Figure 1.** (a) Microscope image of the 4L MoS<sub>2</sub> on Si<sub>3</sub>N<sub>4</sub>, (b) the schematic of the sample, PL spectra of (c) suspended and (d) supported MoS<sub>2</sub> on Si<sub>3</sub>N<sub>4</sub>, and (e) PL peak energy and (f) intensity as a function of layer numbers.

Optical properties of suspended and supported MoS<sub>2</sub> flakes on Si<sub>3</sub>N<sub>4</sub> were investigated using micro-PL spectroscopy. As a function of the number of layers (from a single layer to seven layers) the bandgap of the suspended MoS<sub>2</sub> varies from ~1.90 eV to ~1.35 eV (Figure 1e). Up to 45 meV blueshifts in the PL peak energy were observed in the thicker supported flakes compared to the suspended flakes [38]. There are several studies on the

substrate effect on the optical properties of 2D TMDs in the literature [39–41], although most of these studies were focused on the substrate effect on monolayer TMDs. The weaker, broader, and red-shifted PL from the TMDs transferred onto dielectric substrates can be attributed to the amount of moisture at the interface and/or interlayer charge transfer, which results in charge doping [41–43]. In Figure 1, we observe a consistent reduction in PL intensity for all layer numbers, and a small redshift of the peak energy in the thicker supported flakes compared to the suspended flakes. This can be explained by the possibility of more charge transfer in the thicker layers due to their lower energy bandgap [44].

Next, the effect of UV-O<sub>3</sub> treatment on suspended and supported MoS<sub>2</sub> as a function of number of layers and exposure time was investigated. The main purpose of our study is to understand the layer and substrate dependency of the UV-O<sub>3</sub> treatment time on the optical properties of the 2D TMDs, ideally maintaining their photoluminescence. We chose the UV-O<sub>3</sub> treatment times of 1, 4, 6, and 8 min on each sample. Each sample was exposed separately. Figure 2 shows the PL spectra of pristine and UV-O<sub>3</sub>-treated flakes. As UV-O<sub>3</sub> treatment time increases, the PL intensity decreases for all samples. The intensity of the PL emission from the supported MoS<sub>2</sub> decreases significantly with UV-O<sub>3</sub> treatment time and is eventually fully quenched after 8 min., while the suspended flakes are less affected by the treatment. Figure 3 shows that there are clear differences in the trend between the suspended and supported flakes. In general, the thinner flakes are more sensitive to UV-O<sub>3</sub> treatment for both cases, which is expected; however, for suspended flakes, up to 4 min of exposure for all thicknesses does not degrade the PL intensity significantly. We note that in some layers, the PL intensities after 4 min treatment are even higher than after 1 min treatment time, which is likely due to the small variation in PL intensities between consecutive measurements. The overall trend of above 4 min exposure time is, however, clear.

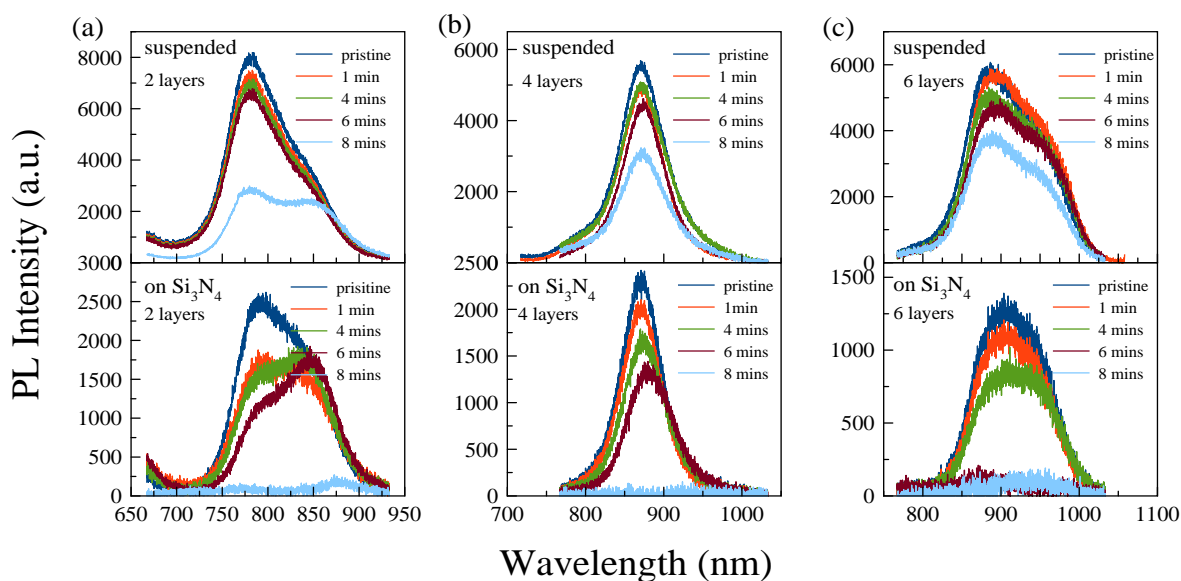


**Figure 2.** PL spectra of (a) two-layer, (b) four-layer, and (c) six-layer MoS<sub>2</sub> flakes with different UV-O<sub>3</sub> treatment times: 1, 4, 6, 8 min.

We use DFT calculations to understand the effect of UV-O<sub>3</sub> on suspended TMDs. Conventional UV-O<sub>3</sub> cleaners have two dominant UV peaks, at 184 nm and 254 nm. Upon irradiation, molecular oxygen (O<sub>2</sub>) present in the air is dissociated by radiation at 184 nm. This results in the formation of two radicals of singlet oxygen (O). These radicals continue to react with molecular oxygens forming molecules of ozone (O<sub>3</sub>). The simulations were carried out for these three species. Sulphur substitutional defects involving these species, as well as surface adsorption onto various non-symmetrically equivalent high symmetry sites, were considered. Both substitution and adsorption of O<sub>3</sub> resulted in dissociation into an O

defect and a free  $O_2$  molecule in the vacuum gap, which is therefore equivalent to the O defects. The formation energies were calculated with a constant oxygen chemical potential of half the energy of an oxygen atom, plotted in Figure 4a, which represents the stability of each type of defect as a function of sulphur chemical potential. In both the sulphur-rich and sulphur-poor extremes, no  $O_2$  defects were stable as their formation energies were above zero for all chemical potentials, hence O defects can be concluded to be the most likely defect to form in this system. In the sulphur-poor region,  $O_2/S$  substitution is the most stable, and for all chemical potentials, O adsorption is the most stable scenario. Figure 4b shows that the unoccupied electronic states introduced by all these defects are higher in energy than the conduction band minimum (CBM) of pristine monolayer  $MoS_2$ , meaning no PL shift should be induced by the defects. The  $O_2$  defects have higher formation energy than the O defects, which indicates that they are likely to be short-lived; however, these short-lived  $O_2$  defects could be relevant for providing mechanisms to form O defects. In Figure 4c, the excess Bader charge was shown as a function of the vertical position of each atom in the unit cell in the case of O adsorption and with one added electron. Low localization can be seen at both top and bottom surfaces, with the most localization on the sulphur atom closest to the adsorbed O atom. Even this larger localization is only 0.08 e, suggesting this localization is extremely weak and unlikely to trap enough charge to cause p-type doping. One singlet O adsorption between the TMD layers was also investigated at the PBE level (the lower level of theory) for both neutral and +1 electron systems. This gave similar charge densities and defect levels compared to O adsorption on the surface. We also note here that our DFT model reflects the substitution of one sulphur atom in the unit cell (Figure 4c), and the adsorption of one of the three oxygen species ( $O$ ,  $O_2$ , and  $O_3$ ) in the suspended 4L  $MoS_2$  system; it does not reflect multiple species adsorption or substitution of multiple sulphur atoms, which potentially happens with longer UV- $O_3$  treatment time. The PL results from short-time UV- $O_3$  treatment (1 to 4 min) show no significant reduction in the intensity nor any peak wavelength shift, which is consistent with our DFT results.

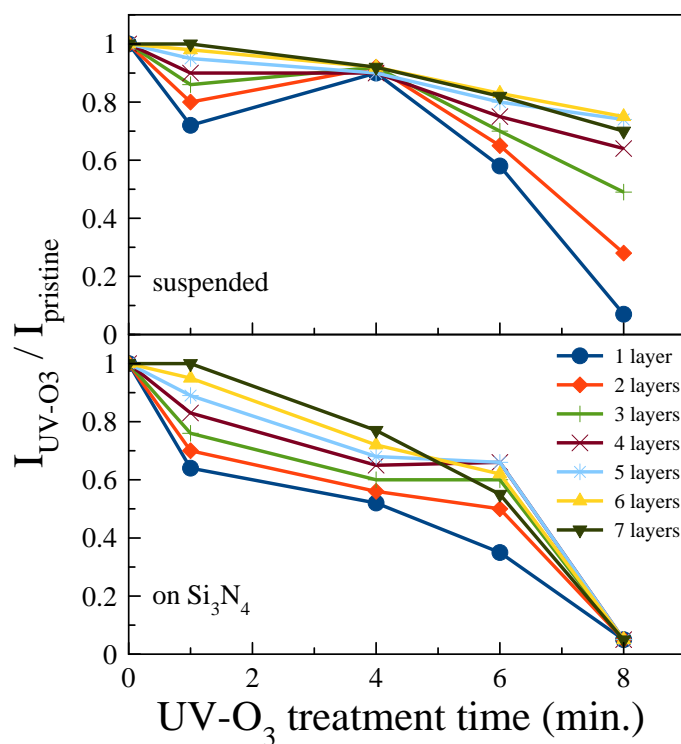
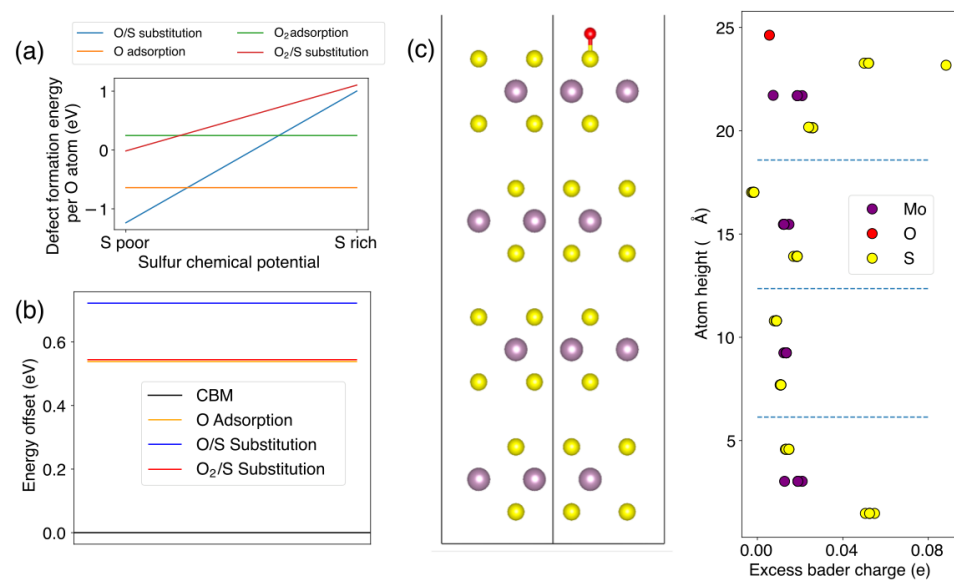


Figure 3. PL intensity ratio as a function of UV- $O_3$  exposure time.



**Figure 4.** (a) Defect formation energies for O (yellow line) and O<sub>2</sub> (green line) adsorption and S (blue and red lines) substitutional defects as a function of sulphur chemical potential; (b) defect energy level offsets for each stable defect mechanism, with respect to the conduction band minimum (CBM, black line) in the pristine 4L-MoS<sub>2</sub> system; (c) excess Bader charge for each atomic site (right), with sites aligned vertically with unit cell (left) for the O adsorption case with the presence of one added electron.

Inclusion of the substrate in the DFT calculations is too computationally time-consuming using the hybrid level of theory and requires taking into account extra parameters, such as surface roughness, optical interferences specifically on dielectric substrates, defects, and impurities on the interface, etc., which is considered to be future work.

To understand the effect of UV-O<sub>3</sub> on the substrate-supported flakes, we analyzed the PL spectra of the 2L and 6L flakes in depth. The reduction in the PL intensities starts from higher energy on the supported 2L and 6L flakes with up to 6 min of UV-O<sub>3</sub> treatment (see Figure 2a,c). This can be explained by carrier dynamics involving the presence of the Si<sub>3</sub>N<sub>4</sub> substrate. The bandgap and photogenerated charge carriers of the substrate under UV irradiation play a key role in this process. The bandgap of the Si<sub>3</sub>N<sub>4</sub> is ~5 eV. During the UV-O<sub>3</sub> exposure, the 184 nm characteristic radiation of the UV source can generate free electrons and holes in the substrate. The generated free electrons diffuse to MoS<sub>2</sub>, which has a lower energy level than that of the conduction band of Si<sub>3</sub>N<sub>4</sub> in the heterostructure (illustrated in Figure 5a). Such diffusion compensates for the decreased electron density caused by the oxygen adsorption and allows more oxygen defect formation on the MoS<sub>2</sub> surface. The transferred electrons also recombine with free holes in MoS<sub>2</sub>, resulting in non-radiative recombination at the interfaces of the flake and the substrate, hence further reduction in the PL intensity of the supported MoS<sub>2</sub>. Moreover, we observed an 11 meV redshift in the PL peak energy of the 4L supported flakes, compared to the suspended 4L flakes, which supports the substrate-induced charge carrier dynamics interpretation. Such substrate-dependent carrier dynamics have been observed previously in graphene [24].

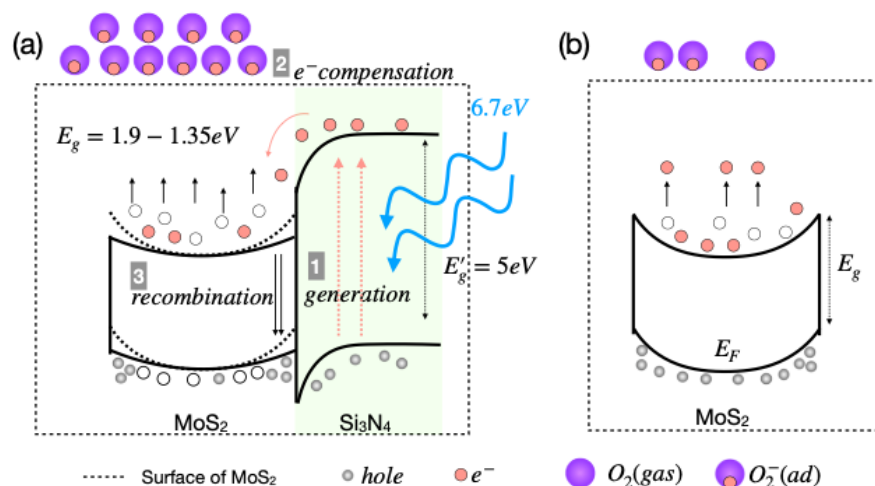


Figure 5. Illustrations of UV-O<sub>3</sub> treatment effect on (a) supported and (b) suspended MoS<sub>2</sub>.

Finally, we fabricated a substrate-supported field effect transistor with a TLM structure using 4L MoS<sub>2</sub> to investigate the doping effect of the UV-O<sub>3</sub> treatment. The optical microscope image and illustrations of the fabricated device are presented in Figure 6a. The structure includes five transistors with different channel lengths from 2 μm to 4 μm in 0.5 μm step, and the consecutive two electrodes can be used as source and drain. The channel width of the transistors is 12 μm. All transistors (with different channel lengths) exhibit the same trend of the input and output characteristics against UV-O<sub>3</sub> treatment. We present the 4 μm length device in detail, in Figure 6b–d, as a function of UV-O<sub>3</sub> treatment time. Figure 6b shows the input characteristic of the transistor.

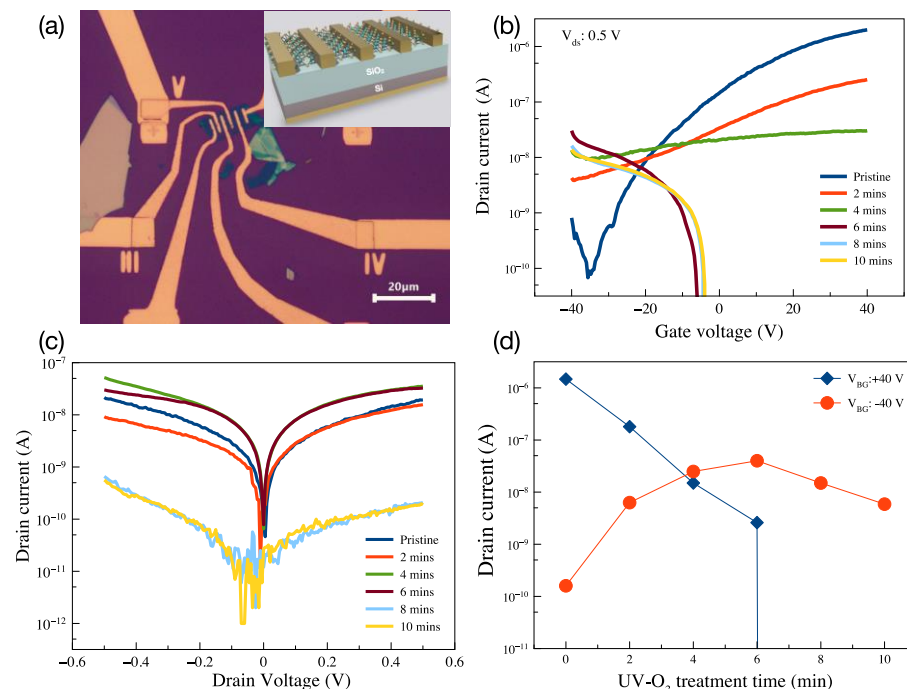


Figure 6. (a) Optical microscope image with 20 μm of a scale bar and illustration (inserted) of the MoS<sub>2</sub> FET, drain-source current as a function of (b) applied gate voltage, (c) applied drain-source voltage, and (d) UV-O<sub>3</sub> treatment time.

The pristine MoS<sub>2</sub> transistor shows n-type dominant ambipolar characteristics; with increasing the UV-O<sub>3</sub> treatment time, the n-type dominance reduces and eventually, the characteristic changes from electron dominant to hole dominant, as seen in Figure 6b,c.



With 6 min treatment time, the on/off ratio for the n-type dominant reduced from  $10^4$  to zero, while that of the p-type dominant increased from 1 to  $10^3$  under 0.5 V bias. On the other hand, when above 6 min of UV-O<sub>3</sub> treatment, not only is the electron density reduced but so is the hole density, and the drain-source current is two orders of magnitude lower after 8- and 10-min of treatment (Figure 6d).

#### 4. Conclusions

The effect of UV-O<sub>3</sub> treatment on the optical and electrical properties of mono- and multi-layer MoS<sub>2</sub> is presented. The PL intensity from substrate-supported MoS<sub>2</sub> decreases significantly with UV-O<sub>3</sub> treatment time and is fully quenched after 8 min of treatment. The PL of suspended flakes is, however, less affected by the UV-O<sub>3</sub> treatment. Our DFT results suggest that no significant charge trapping or PL peak energy shift should be expected from the substitution and adsorption of O, O<sub>2</sub>, and O<sub>3</sub> on the surface of a suspended MoS<sub>2</sub> flake. We conclude that the substrate plays a critical role in the UV-O<sub>3</sub>-induced manipulation of the electrical and optical properties of MoS<sub>2</sub>. The effect of UV-O<sub>3</sub> treatment is also layer-thickness dependent; while the thinner flakes could experience a 90% reduction in the PL intensity, the thicker suspended flakes remain above 60% of their original intensity. Our electrical measurements show that above 6 min of UV-O<sub>3</sub> treatment not only causes a reduction in the electron density but it also deteriorates the hole transport. Our work suggests that 4 min UV-O<sub>3</sub> treatment is the optimum time to produce p-type MoS<sub>2</sub> and maintain above 80% of PL intensity without any shift in emission wavelength. Longer than 4 min leads to deterioration of both optical and electrical properties, which should be taken into consideration in future device fabrication processes.

**Author Contributions:** F.S. and Y.W. fabricated the samples and performed the photoluminescence measurements. A.J.A. performed the DFT calculations, supervised by K.P.M., F.S., Y.K.B. and E.K. fabricated the sample for the electrical characterisation and performed the measurements. F.S., A.J.A., Y.W., K.P.M. and A.E. analyzed the results. F.S., A.E., K.P.M. and Y.W. managed various aspects and funded the project. F.S., A.J.A. and Y.W. wrote the manuscript with contributions from all co-authors. Y.W. oversaw the entire project. All authors have read and agreed to the published version of the manuscript.

**Funding:** This research was funded by the Royal Academy of Engineering (Research Fellowship awarded to Y.W., RF\201718\17131), the Scientific Research Projects Coordination Unit of Istanbul University (FBA-2023-39412, FBG-2022-38573, FBG-2021-37896), the Scientific and Technological Research Council of Turkey (TUBITAK) project (121F169), and EPSRC (EP/R029431 and EP/X035859).

**Data Availability Statement:** The authors declare that all the data and code supporting the findings of this study are available within the article, or upon request from the corresponding author.

**Acknowledgments:** A.J.A. and K.P.M. acknowledge the grant of computing time on ARCHER2 via our membership of the UK's HEC Materials Chemistry Consortium.

**Conflicts of Interest:** The authors declare no conflict of interest.

#### References

1. Fang, H.; Liu, J.; Li, H.; Zhou, L.; Liu, L.; Li, J.; Wang, X.; Krauss, T.F.; Wang, Y. 1305 nm Few-Layer MoTe<sub>2</sub>-on-Silicon Laser-Like Emission. *Laser Photon. Rev.* **2018**, *12*, 1800015. [[CrossRef](#)]
2. Withers, F.; Del Pozo-Zamudio, O.; Mishchenko, A.; Rooney, A.P.; Gholinia, A.; Watanabe, K.; Taniguchi, T.; Haigh, S.J.; Geim, A.K.; Tartakovskii, A.I.; et al. Light-emitting diodes by band-structure engineering in van der Waals heterostructures. *Nat. Mater.* **2015**, *14*, 301–306. [[CrossRef](#)] [[PubMed](#)]
3. Dong, T.; Simões, J.; Yang, Z. Flexible Photodetector Based on 2D Materials: Processing, Architectures, and Applications. *Adv. Mater. Interfaces* **2020**, *7*, 1901657. [[CrossRef](#)]
4. Datta, I.; Chae, S.H.; Bhatt, G.R.; Tadayan, M.A.; Li, B.; Yu, Y.; Park, C.; Park, J.; Cao, L.; Basov, D.N.; et al. Low-loss composite photonic platform based on 2D semiconductor monolayers. *Nat. Photon.* **2020**, *14*, 256–262. [[CrossRef](#)]
5. Allain, A.; Kis, A. Electron and Hole Mobilities in Single-Layer WSe<sub>2</sub>. *ACS Nano* **2014**, *8*, 7180–7185. [[CrossRef](#)]
6. Qu, D.; Liu, X.; Huang, M.; Lee, C.; Ahmed, F.; Kim, H.; Ruoff, R.S.; Hone, J.; Yoo, W.J. Carrier-Type Modulation and Mobility Improvement of Thin MoTe<sub>2</sub>. *Adv. Mater.* **2017**, *29*, 1606433. [[CrossRef](#)]

7. Pham, V.P.; Yeom, G.Y. Recent Advances in Doping of Molybdenum Disulfide: Industrial Applications and Future Prospects. *Adv. Mater.* **2016**, *28*, 9024–9059. [[CrossRef](#)]
8. Ji, H.G.; Solís-Fernández, P.; Yoshimura, D.; Maruyama, M.; Endo, T.; Miyata, Y.; Okada, S.; Ago, H. Chemically Tuned p- and n-Type WSe<sub>2</sub> Monolayers with High Carrier Mobility for Advanced Electronics. *Adv. Mater.* **2019**, *31*, 1903613. [[CrossRef](#)]
9. Allain, A.; Kang, J.; Banerjee, K.; Kis, A. Electrical contacts to two-dimensional semiconductors. *Nat. Mater.* **2015**, *14*, 1195–1205. [[CrossRef](#)]
10. Sarcan, F.; Fairbairn, N.J.; Zotev, P.; Severs-Millard, T.; Gillard, D.J.; Wang, X.; Conran, B.; Heuken, M.; Erol, A.; Tartakovskii, A.I.; et al. Understanding the impact of heavy ions and tailoring the optical properties of large-area monolayer WS<sub>2</sub> using focused ion beam. *Npj 2D Mater. Appl.* **2023**, *7*, 23. [[CrossRef](#)]
11. Luo, W.; Zhu, M.; Peng, G.; Zheng, X.; Miao, F.; Bai, S.; Zhang, X.; Qin, S. Carrier Modulation of Ambipolar Few-Layer MoTe<sub>2</sub> Transistors by MgO Surface Charge Transfer Doping. *Adv. Funct. Mater.* **2018**, *28*, 1704539. [[CrossRef](#)]
12. Loh, L.; Zhang, Z.; Bosman, M.; Eda, G. Substitutional doping in 2D transition metal dichalcogenides. *Nano Res.* **2021**, *14*, 1668–1681. [[CrossRef](#)]
13. Iqbal, M.; Elahi, E.; Amin, A.; Hussain, G.; Aftab, S. Chemical doping of transition metal dichalcogenides (TMDCs) based field effect transistors: A review. *Superlattices Microstruct.* **2020**, *137*, 106350. [[CrossRef](#)]
14. Xu, K.; Zhao, Y.; Lin, Z.; Long, Y.; Wang, Y.; Chan, M.; Chai, Y. Doping of two-dimensional MoS<sub>2</sub> by high energy ion implantation. *Semicond. Sci. Technol.* **2017**, *32*, 124002. [[CrossRef](#)]
15. Luo, P.; Zhuge, F.; Zhang, Q.; Chen, Y.; Lv, L.; Huang, Y.; Li, H.; Zhai, T. Doping engineering and functionalization of two-dimensional metal chalcogenides. *Nanoscale Horiz.* **2019**, *4*, 26–51. [[CrossRef](#)] [[PubMed](#)]
16. Chen, R.; Liu, Q.; Liu, J.; Zhao, X.; Liu, J.; He, L.; Wang, J.; Li, W.; Xiao, X.; Jiang, C. Design of high performance MoS<sub>2</sub>-based non-volatile memory via ion beam defect engineering. *2D Mater.* **2019**, *6*, 034002. [[CrossRef](#)]
17. Yang, W.; Sun, Q.-Q.; Geng, Y.; Chen, L.; Zhou, P.; Ding, S.-J.; Zhang, D.W. The Integration of Sub-10 nm Gate Oxide on MoS<sub>2</sub> with Ultra Low Leakage and Enhanced Mobility. *Sci. Rep.* **2015**, *5*, 11921. [[CrossRef](#)]
18. Iacovella, F.; Koroleva, A.; Rybkin, A.G.; Fouskaki, M.; Chaniotakis, N.; Savvidis, P.; Deligeorgis, G. Impact of thermal annealing in forming gas on the optical and electrical properties of MoS<sub>2</sub> monolayer. *J. Phys. Condens. Matter* **2021**, *33*, 035001. [[CrossRef](#)]
19. Luo, T.; Pan, B.; Zhang, K.; Dong, Y.; Zou, C.; Gu, Z.; Zhang, L. Electron beam lithography induced doping in multilayer MoTe<sub>2</sub>. *Appl. Surf. Sci.* **2021**, *540*, 148276. [[CrossRef](#)]
20. Liang, Q.; Gou, J.; Arramel; Zhang, Q.; Zhang, W.; Wee, A.T.S. Oxygen-induced controllable p-type doping in 2D semiconductor transition metal dichalcogenides. *Nano Res.* **2020**, *13*, 3439–3444. [[CrossRef](#)]
21. Vig, J.R. UV/ozone cleaning of surfaces. *J. Vac. Sci. Technol. A* **1985**, *3*, 1027–1034. [[CrossRef](#)]
22. Li, W.; Liang, Y.; Yu, D.; Peng, L.; Pernstich, K.P.; Shen, T.; Walker, A.R.H.; Cheng, G.; Hacker, C.A.; Richter, C.A.; et al. Ultraviolet/ozone treatment to reduce metal-graphene contact resistance. *Appl. Phys. Lett.* **2013**, *102*, 183110. [[CrossRef](#)]
23. Chen, C.W.; Ren, F.; Chi, G.-C.; Hung, S.-C.; Huang, Y.P.; Kim, J.; Kravchenko, I.I.; Pearton, S.J. UV ozone treatment for improving contact resistance on graphene. *J. Vac. Sci. Technol. B* **2012**, *30*, 060604. [[CrossRef](#)]
24. Liu, L.; Cao, Z.; Wang, W.; Wang, E.; Cao, Y.; Zhan, Z. Substrate-dependent resistance decrease of graphene by ultraviolet-ozone charge doping. *RSC Adv.* **2016**, *6*, 62091–62098. [[CrossRef](#)]
25. Zheng, X.; Zhang, X.; Wei, Y.; Liu, J.; Yang, H.; Zhang, X.; Wang, S.; Xie, H.; Deng, C.; Gao, Y.; et al. Enormous enhancement in electrical performance of few-layered MoTe<sub>2</sub> due to Schottky barrier reduction induced by ultraviolet ozone treatment. *Nano Res.* **2020**, *13*, 952–958. [[CrossRef](#)]
26. Yang, H.I.; Park, S.; Choi, W. Modification of the optoelectronic properties of two-dimensional MoS<sub>2</sub> crystals by ultraviolet-ozone treatment. *Appl. Surf. Sci.* **2018**, *443*, 91–96. [[CrossRef](#)]
27. Jung, C.; Yang, H.I.; Choi, W. Effect of Ultraviolet-Ozone Treatment on MoS<sub>2</sub> Monolayers: Comparison of Chemical-Vapor-Deposited Polycrystalline Thin Films and Mechanically Exfoliated Single Crystal Flakes. *Nanoscale Res. Lett.* **2019**, *14*, 2788. [[CrossRef](#)]
28. Kang, M.; Yang, H.I.; Choi, W. Oxidation of WS<sub>2</sub> and WSe<sub>2</sub> monolayers by ultraviolet-ozone treatment. *J. Phys. D Appl. Phys.* **2019**, *52*, 505105. [[CrossRef](#)]
29. Zheng, X.; Wei, Y.; Liu, J.; Wang, S.; Shi, J.; Yang, H.; Peng, G.; Deng, C.; Luo, W.; Zhao, Y.; et al. A homogeneous p–n junction diode by selective doping of few layer MoSe<sub>2</sub> using ultraviolet ozone for high-performance photovoltaic devices. *Nanoscale* **2019**, *11*, 13469–13476. [[CrossRef](#)]
30. Kresse, G.; Hafner, J. *Ab initio* molecular dynamics for liquid metals. *Phys. Rev. B* **1993**, *47*, 558–561. [[CrossRef](#)]
31. Kresse, G.; Furthmüller, J. Efficiency of ab-initio total energy calculations for metals and semiconductors using a plane-wave basis set. *Comput. Mater. Sci.* **1996**, *6*, 15–50. [[CrossRef](#)]
32. Kresse, G.; Furthmüller, J. Efficient iterative schemes for *ab initio* total-energy calculations using a plane-wave basis set. *Phys. Rev. B* **1996**, *54*, 11169–11186. [[CrossRef](#)]
33. Perdew, J.P.; Levy, M. Physical Content of the Exact Kohn-Sham Orbital Energies: Band Gaps and Derivative Discontinuities. *Phys. Rev. Lett.* **1983**, *51*, 1884–1887. [[CrossRef](#)]
34. Grimme, S.; Antony, J.; Ehrlich, S.; Krieg, H. A consistent and accurate ab initio parametrization of density functional dispersion correction (DFT-D) for the 94 elements H–Pu. *J. Chem. Phys.* **2010**, *132*, 154104. [[CrossRef](#)]

35. Peralta, J.E.; Heyd, J.; Scuseria, G.E.; Martin, R.L. Spin-orbit splittings and energy band gaps calculated with the Heyd-Scuseria-Ernzerhof screened hybrid functional. *Phys. Rev. B* **2006**, *74*, 073101. [[CrossRef](#)]
36. Ganose, A.M.; Jackson, A.J.; Scanlon, D.O. sumo: Command-line tools for plotting and analysis of periodic ab initio calculations. *J. Open Source Softw.* **2018**, *3*, 717. [[CrossRef](#)]
37. Armstrong, A.; McKenna, K.; Wang, Y. Directional dependence of band gap modulation via uniaxial strain in MoS<sub>2</sub> and TiS<sub>3</sub>. *Nanotechnology* **2023**, *35*, 015704. [[CrossRef](#)]
38. Mak, K.F.; Lee, C.; Hone, J.; Shan, J.; Heinz, T.F. Atomically Thin MoS<sub>2</sub>: A New Direct-Gap Semiconductor. *Phys. Rev. Lett.* **2010**, *105*, 136805. [[CrossRef](#)]
39. Lippert, S.; Schneider, L.M.; Renaud, D.; Kang, K.N.; Ajayi, O.; Kuhnert, J.; Halbich, M.-U.; Abdulmunem, O.M.; Lin, X.; Hassoon, K.; et al. Influence of the substrate material on the optical properties of tungsten diselenide monolayers. *D Mater.* **2017**, *4*, 025045. [[CrossRef](#)]
40. Buscema, M.; Steele, G.A.; van der Zant, H.S.J.; Castellanos-Gomez, A. The effect of the substrate on the Raman and photoluminescence emission of single-layer MoS<sub>2</sub>. *Nano Res.* **2014**, *7*, 561–571. [[CrossRef](#)]
41. Chae, W.H.; Cain, J.D.; Hanson, E.D.; Murthy, A.A.; Dravid, V.P. Substrate-induced strain and charge doping in CVD-grown monolayer MoS<sub>2</sub>. *Appl. Phys. Lett.* **2017**, *111*, 143106. [[CrossRef](#)]
42. Amani, M.; Chin, M.L.; Mazzoni, A.L.; Burke, R.A.; Najmaei, S.; Ajayan, P.M.; Lou, J.; Dubey, M. Growth-substrate induced performance degradation in chemically synthesized monolayer MoS<sub>2</sub> field effect transistors. *Appl. Phys. Lett.* **2014**, *104*, 203506. [[CrossRef](#)]
43. Kung, Y.; Hosseini, N.; Dumcenco, D.; Fantner, G.E.; Kis, A. Air and Water-Stable n-Type Doping and Encapsulation of Flexible MoS<sub>2</sub> Devices with SU8. *Adv. Electron. Mater.* **2019**, *5*, 1800492. [[CrossRef](#)]
44. Iqbal, M.W.; Shahzad, K.; Akbar, R.; Hussain, G. A review on Raman finger prints of doping and strain effect in TMDCs. *Microelectron. Eng.* **2019**, *219*, 111152. [[CrossRef](#)]

**Disclaimer/Publisher's Note:** The statements, opinions and data contained in all publications are solely those of the individual author(s) and contributor(s) and not of MDPI and/or the editor(s). MDPI and/or the editor(s) disclaim responsibility for any injury to people or property resulting from any ideas, methods, instructions or products referred to in the content.